# Step Coalescence by Collective Motion at an Incommensurate Grain Boundary

M. L. Bowers,[1] C. Ophus,[1] A. Gautam,[1] F. Lançon,[2] and U. Dahmen[1]
[1]Molecular Foundry, National Center for Electron Microscopy, LBNL, Berkeley, California 94720, USA
[2]Université Grenoble Alpes, 38042 Grenoble, France, and INAC, SP2M, L_sim, CEA, 38054 Grenoble, France
(Received 11 September 2015; revised manuscript received 25 October 2015; published 9 March 2016)

Using extended time series scanning transmission electron microscopy, we investigate structural fluctuations at an incommensurate grain boundary in Au. Atomic-resolution imaging reveals the coalescence of two interfacial steps, or disconnections, of different height via coordinated motion of atoms along close-packed directions. Numerical simulations uncover a transition pathway that involves constriction and expansion of a characteristic stacking fault often associated with grain boundaries in face-centered cubic materials. It is found that local atomic fluctuations by enhanced point defect diffusion may play a critical role in initiating this transition. Our results offer new insights into the collective motion of atoms underlying the lateral advance of steps that control the migration of faceted grain boundaries.

DOI: 10.1103/PhysRevLett.116.106102

Grain boundaries in crystalline materials are critically important for macroscopic properties such as strength, electronic transport, corrosion resistance, and creep [1–3]. To enhance these properties, processing techniques are therefore often aimed at modifying the existing grain boundary content via processes such as recrystallization and grain growth. While much is known about the structural character of grain boundaries and the variables that affect their mobility, e.g., Ref. [4], the atomic-scale mechanisms of migration are still poorly understood. Several experimental studies suggest that cooperative, stringlike motion of groups of atoms is a primary mechanism of grain boundary migration [5–7]. Molecular dynamics (MD) simulations indicate that such atomic cascade events can be triggered by local volume fluctuations at the grain boundary and may occur in the absence of an external driving force [8–10]. Furthermore, the effect of an applied shear stress on the migration of a symmetrical grain boundary in Cu has recently been simulated by MD, revealing the detailed role of steps in the mechanism of motion [11]. However, a direct, quantitative comparison of experimental observations and atomistic simulations has only recently become possible due to advances in aberration-corrected electron microscopy and image analysis.

The spatial and temporal resolution attainable with modern microscopes [12], coupled with recently developed computational methods for detecting and quantifying structural fluctuations [13], enables an unprecedented view of stochastic interface dynamics. Experimental images can be used to build energy-minimized input structures, while molecular dynamics reveals the lowest energy pathway between these observed states. This provides a snapshot of transient activated states whose time scale is well beyond the temporal resolution of experiment. These intermediate configurations provide a deeper understanding of the atomic mechanisms of step motion in the migration of grain boundaries.

In this work, we investigate the role of cooperative motion in step propagation at a $\{001\}/\{110\}$ grain boundary in a 90° $\langle 110\rangle$ gold bicrystal. This interface is termed "incommensurate" since the ratio of plane spacings meeting across the boundary is irrational, which has important implications for grain boundary behavior [14]. The migration mechanisms of these boundary segments are of unique interest due to their observed role in island grain shrinkage, where $\{001\}/\{110\}$ facets are observed to be one of three preferred boundary inclinations as the grain shrinks and the degree of anisotropy increases [15]. Notably, these facets were observed to be the least mobile of the three, remaining stationary for long periods followed by erratic bursts of motion mediated by step nucleation and propagation. Other work suggests that the mobility of these facets depends strongly on interactions with free surfaces, as this particular interface can exhibit a chevronlike dissociation when it intersects a surface [16,17].

In an effort to observe structural changes associated with the $\{001\}/\{110\}$ boundary, extended time series high angle annular dark field scanning transmission electron microscopy (HAADF-STEM) was performed on bicrystalline Au thin films. The films were grown by physical vapor deposition on $\{001\}$ Ge substrates, resulting in a mazed bicrystal structure consisting of two columnar $\{110\}$ Au variants rotated 90° about a common $\langle 110\rangle$ axis [16,18]. The substrate was subsequently etched away to create free standing Au films less than 4 nm thick for characterization. These specimens are ideal for studying structural fluctuations around equilibrium due to the absence of strain and surface energy as possible driving forces for boundary migration. Therefore, the ambient temperature dynamic events observed in this study are induced purely by the electron beam and are expected to play a key role in thermal processes such as grain growth. Although the 300 kV electrons used for imaging are well below the knock-on

 

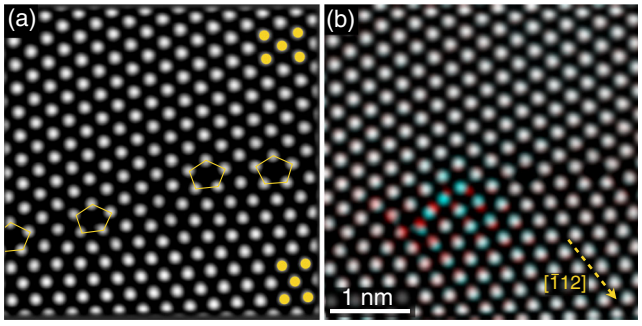


FIG. 1. (a) Intensity average of several HAADF-STEM fast scan images showing a {001}/{110} boundary containing two steps. Fivefold structural units are outlined in yellow. (b) Colored composite image of averaged intensities before and after a structural event to highlight the atomic displacements.

threshold for Au [19], they are able to transfer sufficient energy to induce structural changes and enhance diffusion.

HAADF-STEM imaging was performed at 300 kV on the aberration-corrected TEAM 0.5 microscope at the National Center for Electron Microscopy with imaging conditions tuned to fully correct for aberrations up to third order. A dwell time of 0.5 $\mu$s and a probe current of 100 pA were chosen to optimize the signal-to-noise ratio and to provide sufficient temporal resolution (~8 fps at 512 × 512 pixels) to observe dynamic structural changes. A time domain edge detection algorithm was used to identify stochastic structural fluctuations, and cumulative averaging of images between events allowed accurate quantitative comparison with atomistic simulations [13]. Figure 1(a) shows an intensity averaged image from several consecutive frames of typical {001}/{110} grain boundary segments separated by steps perpendicular to the boundary plane. The lattice periodicities of the two grains along the incommensurate direction are in the ratio of $1:\sqrt{2}$, and the fivefold structural units that characterize this boundary are highlighted.

A multitude of such boundaries were studied in an effort to detect stochastic events occurring at the interface. Figure 1(b) illustrates one such occurrence via a colored overlay of event-averaged atomic resolution micrographs before and after the structural change. The result is a composite image where red and cyan represent atomic column positions before and after the event, respectively, and white represents columns that remain stationary. This clearly shows the coordinated shuffle of atoms along close-packed ⟨112⟩ directions during the structural transition that ultimately leads to the advance of the lower grain. After several seconds, the boundary returns to its original configuration, suggesting that this is a reversible fluctuation about equilibrium [7]. Notably, the identical structure and transition path shown in Fig. 1(b) have been observed in multiple specimens, indicating that this particular rearrangement may represent an important boundary migration mechanism. For a movie of the dynamic STEM observation of this structural fluctuation, see Ref. [20].

The collective motion observed in Fig. 1(b) modifies the step configuration as the boundary advances. To clearly understand this migration mechanism, it is useful to characterize the interfacial steps by their extent into each crystal. In the following discussion, grain boundary steps will be described by the number of planes parallel to the boundary in each grain that meet edge to edge at the step. A step that contains $n$ {100} planes in the lower grain and $m$ {110} planes in the upper grain will be denoted $n|m$ [21]. Using this notation, the atomic shuffle allows a 1|1 and a 2|3 step to coalesce into a 3|4 step, as can be seen in Figs. 2(a) and 2(c),

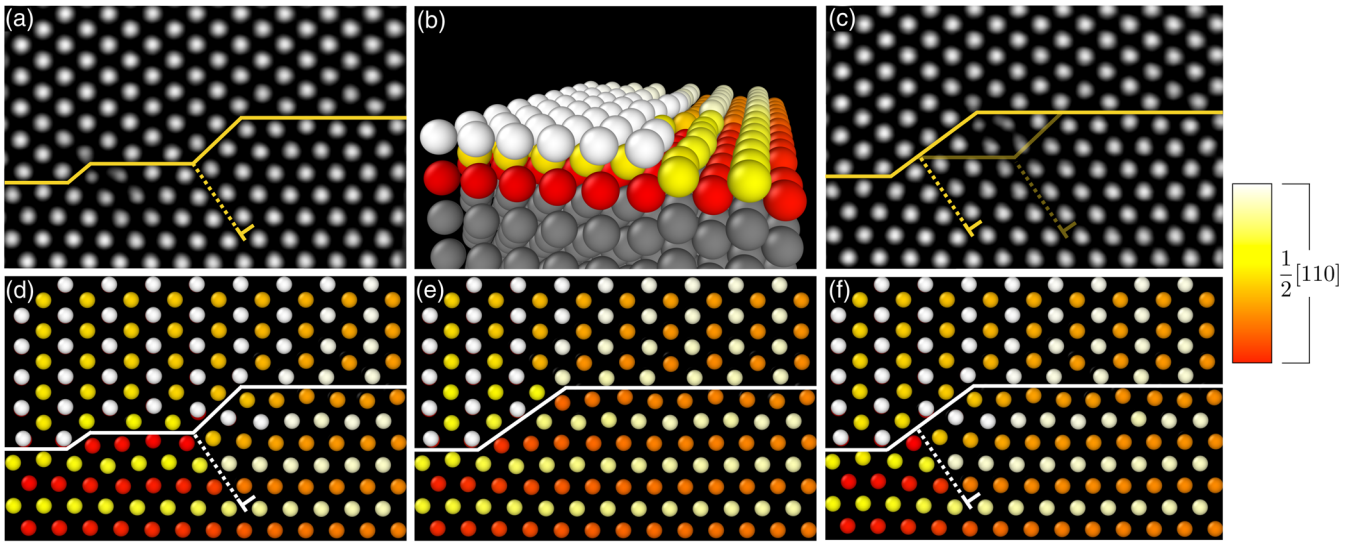


FIG. 2. [110] projections of the experimental (a) and simulated (d) initial boundary configuration with 1|1 and 2|3 steps, simulated saddle point configuration (e), and experimental (c) and simulated (f) final configuration with a 3|4 step. All simulations are color-coded for atomic position along the [110] direction, as shown in the perspective view of the initial configuration (b). Dotted lines indicate stacking faults and the color legend describes a $\frac{1}{2}$[110] period.

where the interface is highlighted before and after the transition.

The mechanism of the transition was explored in detail using numerical simulation techniques. Energy-minimized structural models of the initial and final configurations were built to mirror the experimental observations and a minimum-energy pathway [22,23] between the two structures was calculated. The limited volume of material involved in the transition enables a direct comparison to atomistic simulations done with an $N$-body interatomic potential [24] and using a realistic cell size. Finite-length grain boundaries of perfect crystals were shifted orthogonally to the interface to create the unrelaxed step configurations. A cylinder 23.6 nm in diameter and 3.45 nm in height, parallel to the common $\langle 110 \rangle$ axis and containing 89 780 atoms, was centered at the step location. Free boundary conditions were applied at its surface. The total potential energy was minimized and the two resulting configurations are shown in Figs. 2(d) and 2(f). An initial path through the configuration space was then computed by linear interpolation between the two configurations. This path was iteratively optimized [22] to be orthogonal to the isoenergy manifolds of the configuration space. The result is a minimum-energy pathway going through a main saddle-point configuration but also through secondary minima and saddle points. Figure 3 shows the energy variation of the Au film during the transition when 241 configurations are used to represent the path during its calculation. The energy barrier obtained from this calculation ($\Delta E_{\max}$) is ~0.42 eV. Additionally, the simulations indicate that approximately 220 atoms move by more than 50 pm during the collective motion that leads to step coalescence. Figure 4 shows atoms that have undergone significant displacement during this event. This behavior is in line with observations by Merkle *et al.* [6], who reported reversible collective effects involving 150–300 atoms.

The simulated transition path provides insight into the mechanism of the observed transition by revealing atomic trajectory information beyond the temporal resolution of the experiment. In particular, it uncovers an intermediate configuration associated with the saddle point of the energy curve in Fig. 3 that is critical to understanding the defect reactions that lead to step coalescence. A [110] projection of this intermediate state is shown in Fig. 2(e), along with projections of the initial [Fig. 2(d)] and final [Fig. 2(f)] configurations for comparison to experiment. Close inspection of the transition pathway indicates the following sequence of events: (1) the stacking fault attached to the 2|3 step constricts until it is contained within the boundary plane; (2) the 2|3 step moves toward the 1|1 step, coalescing into a 3|4 step; (3) a stacking fault attached to the 3|4 step expands into the lower grain. For a movie containing all 241 MD configurations rendered in Ovito [25], see Ref. [20]. The simulation cell has been color-coded by centrosymmetry parameter [26] to highlight the grain boundary and stacking fault over the course of the transition.

A structural analysis of this interfacial defect reaction requires the concept of disconnections [27,28]. Disconnections have both a step component $\boldsymbol{t}$ and a dislocation component with Burgers vector $\boldsymbol{b}$, and are important defects in accommodating interface structure [21,29]. All steps present in this case contain a small edge dislocation component, and steps with a mixed parity $n|m$ ratio, e.g., 2|3 and 3|4, also contain a screw component of $\frac{1}{4}[110]$. The screw dislocation is necessary to maintain the $\ldots abab \ldots$ stacking along the [110] direction at the interface on both sides of the step. Since atomic stacking along the direction of projection is impossible to visualize experimentally, the first few layers of Figs. 2(d)–2(f) have been color coded by height along [110]. The white-red gradient describes a full $\frac{1}{2}[110]$ period, which is shown more clearly in the perspective view of Fig. 2(b). To maintain proper stacking at the two boundary segments separated by the disconnection, the atoms to the left of the

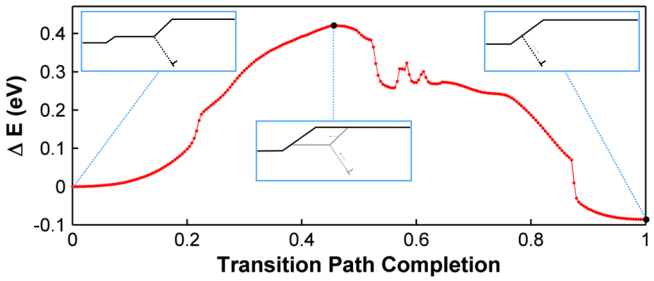


FIG. 3. Energy variation $\Delta E$ of the Au film for 241 simulated atomic configurations along the transition path between initial ($x = 0$) and final ($x = 1$) observed structures. Insets show schematic views of the corresponding structure at end points and maximum total energy.

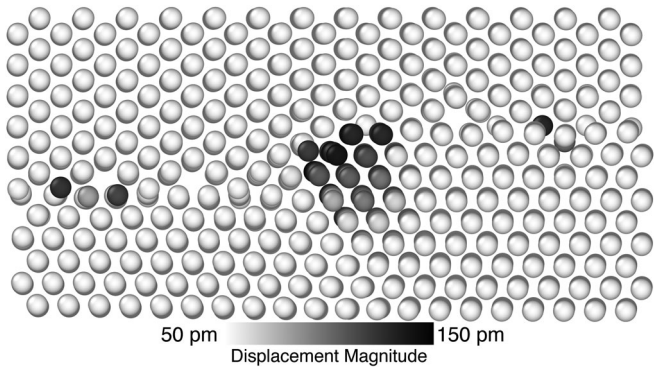


FIG. 4. Simulated step configuration showing the displacement magnitude of atoms during the transition. Shaded atoms have moved by more than 50 pm. (Note that the few outliers visible in this figure are surface atoms whose positions are highly sensitive to small grain shifts associated with the coordinated shuffle.)

mixed parity steps in Figs. 2(d) and 2(f) are shifted downward by $\frac{1}{4}[110]$. This is initially accommodated by the stacking fault extending into the lower grain. The component of this $\frac{1}{6}\langle 121\rangle$ Shockley partial, resolved along the $\langle 110\rangle$ tilt axis, is $\frac{1}{4}\langle 110\rangle$.

While the stacking fault creates a favorable stacking sequence at the interface, it also pins the step in place, preventing it from shifting laterally along the boundary. Similar to the constriction of stacking fault segments to enable cross slip, this relaxed boundary configuration must become compact before the 1|1 and 2|3 steps can merge. Inspection of the MD transition pathway suggests that constriction of this stacking fault is initiated by a kink at the surface, which propagates along the [110] direction until the $\frac{1}{4}[110]$ screw dislocation is confined to the step plane. This can be seen in Fig. 2(e), where the change in column height (indicated by color) is gradual over the span of the step, instead of being confined to a single $\{111\}$ interplanar spacing as in Figs. 2(d) and 2(f). Given an experimental stacking fault energy of 32 $mJ/m^2$ for Au [30], the energy required for constriction of a 1 nm stacking fault in a 3.45 nm thick film is ~0.69 eV. Although the energetics of the transition are complex, this is of the same order of magnitude as the total energy barrier of ~0.42 eV obtained from simulation of a slab with the same thickness. It should be noted that, although discussed as separate events, the constriction of the stacking fault followed by lateral motion of the 2|3 step occurs as part of a single collective rearrangement of atoms.

Other observations of similar grain boundary segments suggest that the dislocation content of mixed parity steps is not always accommodated by the emission of a stacking fault. It is likely that the relaxation observed in this case is related to the precise inclination of the step itself. Experimental and computational studies have confirmed that many interfaces in low stacking fault energy metals relax by widening the structural extent of the interface through the emission of stacking faults [31–35]. Dissociation of grain boundaries into the so-called 9R structure—a roughly 1 nm thick layer of rhombohedral stacking characterized by an intrinsic stacking fault every third close-packed plane—has been observed experimentally in several systems, including Cu, Ag, and Au [36–38]. Medlin *et al.* observed this particular relaxation in Au at a $\{111\}/\{112\}$ facet [38]. Figure 2 shows that the orientation of the 2|3 and 3|4 facet is precisely this interface. Given the limited length of this facet, a complete 9R stacking sequence is not apparent; however, the stacking faults before and after the structural transition show the characteristic two plane separation of this relaxation and an extent of approximately 1 nm.

Medlin *et al.* attribute the relaxation of the $\{111\}/\{112\}$ facet to the inefficient packing at the interface [38]. Shockley partial dislocations are emitted to increase the packing density at the interface, where a large free volume exists every third plane. The incommensurate $\{001\}/\{110\}$ boundary is characterized by high energy pentagonal units with a large free volume [39], which may play a critical role in initiating the collective motion. As shown in the composite image of Fig. 1(b), as well as the individual configurations in Fig. 2, the mobile region is bounded on either side by these open units. The columns at the base of these units (belonging to the lower grain) show decreased intensity and blurring for several frames before the transition, as shown in Figs. 2(a) and 2(c). This suggests agitation of the atoms where the close-packed planes of the lower grain meet the open units. Additionally, the simulations indicate a large free volume of the atomic column where kink nucleation occurs, which initiates the cooperative shift that leads to step coalescence.

This mechanism agrees with the conclusions of Zhang *et al.*, who used molecular dynamics simulations to show that string-like cooperative motion is triggered by local volume fluctuations at the interface [8,9]. Although these simulations reveal coordinated shuffles both in the plane of the film and parallel to the tilt axis, the in-plane motion was found to be the rate-limiting step in boundary migration. Recent work by Yu *et al.* found that grain boundaries can act as unsaturable vacancy sinks and that a constant vacancy flux gives rise to grain boundary migration in the absence of other driving forces [10]. It is likely that, in conjunction with the free surface, the electron beam can enhance point defect diffusion at the boundary, nucleating the transformation. Thus, the present experimental and simulated observations are consistent with a beam-driven point defect flux at the boundary that triggers kink nucleation and the subsequent cascade event that leads to step coalescence and boundary motion.

In summary, we have identified a mechanism of grain boundary migration via step coalescence. While collective effects and step motion have been observed or simulated previously, a fundamental understanding of the defect reactions and energetics of these events has remained elusive. By combining high resolution dynamic observations and atomistic simulations at the same scale, we have been able to bridge the gap between static and dynamic accounts of interfacial structure. Specifically, we have shown that the cooperative motion of atoms involving the constriction and expansion of characteristic stacking faults allows disconnections in a $\{001\}/\{110\}$ incommensurate grain boundary to merge, leading to the advance of the boundary. Our repeated observation of this and similar dynamic events implies that step coalescence is a critical mechanism of grain boundary motion, with more general relevance for crystalline interfaces. The mechanism reported here is expected to have broad implications for thermally activated grain boundary migration, especially in low stacking fault energy materials such as austenitic stainless steels [40], as well as Cu, Ag, Au, and their alloys [33,41].

Work at the Molecular Foundry was supported by the Office of Science, Office of Basic Energy Sciences, of the U.S. Department of Energy under Contract No. DE-AC02-05CH11231.

[1] A. Sutton and R. Balluffi, *Interfaces in Crystalline Materials* (Clarendon Press, Oxford, 1995).
[2] Y. Mishin, M. Asta, and J. Li, Acta Mater. **58**, 1117 (2010).
[3] K. E. Harris and A. H. King, Acta Mater. **46**, 6195 (1998).
[4] G. Gottstein, U. Czubayko, D. A. Molodov, L. S. Shvindlerman, and W. Wunderlich, Mater. Sci. Forum **204–206**, 99 (1996).
[5] K. L. Merkle and L. J. Thompson, Mater. Lett. **48**, 188 (2001).
[6] K. L. Merkle, L. J. Thompson, and F. Phillipp, Phys. Rev. Lett. **88**, 225501 (2002).
[7] K. L. Merkle, L. J. Thompson, and F. Phillipp, Interface Sci. **12**, 277 (2004).
[8] H. Zhang and D. J. Srolovitz, Acta Mater. **54**, 623 (2006).
[9] H. Zhang, D. J. Srolovitz, J. F. Douglas, and J. A. Warren, Phys. Rev. B **74**, 115404 (2006).
[10] W. Yu and M. Demkowicz, J. Mater. Sci. **50**, 4047 (2015).
[11] A. Rajabzadeh, F. Mompiou, M. Legros, and N. Combe, Phys. Rev. Lett. **110**, 265507 (2013).
[12] D. J. Smith, Micron **43**, 504 (2012).
[13] A. Gautam, C. Ophus, F. Lançon, P. Denes, and U. Dahmen, Ultramicroscopy **151**, 78 (2015).
[14] F. Lançon, J. Ye, D. Caliste, T. Radetic, A. M. Minor, and U. Dahmen, Nano Lett. **10**, 695 (2010).
[15] T. Radetic, C. Ophus, D. L. Olmsted, M. Asta, and U. Dahmen, Acta Mater. **60**, 7051 (2012).
[16] T. Radetic and U. Dahmen, Mater. Res. Soc. Symp. Proc. **695**, 1 (2002).
[17] T. Radetic, F. Lancon, and U. Dahmen, Phys. Rev. Lett. **89**, 085502 (2002).
[18] K. H. Westmacott, S. Hinderberger, and U. Dahmen, Philos. Mag. A **81**, 1547 (2001).
[19] R. F. Egerton, P. Li, and M. Malac, Micron **35**, 399 (2004).
[20] See Supplemental Material at http://link.aps.org/supplemental/10.1103/PhysRevLett.116.106102 for movies of dynamic STEM observations and corresponding simulated transition path.
[21] R. C. Pond, D. L. Medlin, and A. Serra, Philos. Mag. **86**, 4667 (2006).
[22] A. Ulitsky and R. Elber, J. Chem. Phys. **92**, 1510 (1990).
[23] G. Henkelman and H. Jónsson, J. Chem. Phys. **113**, 9978 (2000).
[24] T. Deutsch, P. Bayle, F. Lancon, and J. Thibault, J. Phys. Condens. Matter **7**, 6407 (1995).
[25] A. Stukowski, Modelling Simul. Mater. Sci. Eng. **18**, 015012 (2009).
[26] C. L. Kelchner, S. J. Plimpton, and J. C. Hamilton, Phys. Rev. B **58**, 11085 (1998).
[27] R. C. Pond, in *Dislocations in Solids* (Elsevier, North Holland, 1989),Vol. 8, pp. 1–66.
[28] A. Rajabzadeh, F. Mompiou, S. Lartigue-Korinek, N. Combe, M. Legros, and D. A. Molodov, Acta Mater. **77**, 223 (2014).
[29] J. Hirth and R. Pond, Acta Metall. **44**, 4749 (1996).
[30] J. Hirth and J. Lothe, *Theory of Dislocations*, 2nd ed. (Wiley, New York, 1982).
[31] W. Krakow and D. Smith, Ultramicroscopy **22**, 47 (1987).
[32] K. L. Merkle, Ultramicroscopy **37**, 130 (1991).
[33] J. D. Rittner, D. N. Seidman, and K. L. Merkle, Phys. Rev. B **53**, R4241 (1996).
[34] J. D. Rittner and D. N. Seidman, Phys. Rev. B **54**, 6999 (1996).
[35] J. A. Brown and Y. Mishin, Phys. Rev. B **76**, 134118 (2007).
[36] F. Ernst, M. W. Finnis, D. Hofmann, T. Muschik, U. Schönberger, U. Wolf, and M. Methfessel, Phys. Rev. Lett. **69**, 620 (1992).
[37] U. Wolf, F. Ernst, T. Muschik, M. W. Finnis, and H. F. Fischmeister, Philos. Mag. A **66**, 991 (1992).
[38] D. L. Medlin, S. M. Foiles, and D. Cohen, Acta Mater. **49**, 3689 (2001).
[39] A. Gautam, C. Ophus, F. Lancon, V. Radmilovic, and U. Dahmen, Acta Mater. **61**, 5078 (2013).
[40] L. Vitos, J.-O. Nilsson, and B. Johansson, Acta Mater. **54**, 3821 (2006).
[41] W. Li, S. Lu, Q.-M. Hu, S. K. Kwon, B. Johansson, and L. Vitos, J. Phys. Condens. Matter **26**, 265005 (2014).